Computer Methods and Programs in Biomedicine 219 (2022) 106742

Contents lists available at ScienceDirect

Computer Methods and Programs in Biomedicine

journal homepage: www.elsevier.com/locate/cmpb

Health classification of Meibomian gland images using keratography 5M based on AlexNet model

Xianxian Luo[a,b], Wenghao Wen[a,b], Jingru Wang[c], Songya Xu[d], Yingying Gao[c,*], Jianlong Huang[a,b]

[a] Faculty of Mathematics and Computer Science, Quanzhou Normal University, Quanzhou 362000, China
[b] Fujian Provincial Key Laboratory of Data Intensive Computing, Quanzhou 362000, China
[c] Department of Ophthalmology, 2nd Affiliated Hospital, Fujian Medical University, Quanzhou 362000, China
[d] Faculty of Educational Science, Quanzhou Normal University, Quanzhou 362000, China

ARTICLE INFO

Article history:
Received 14 October 2021
Revised 28 February 2022
Accepted 9 March 2022

Keywords:
Meibomian gland dysfunction
Deep learning
AlexNet
Keratography 5M
Ophthalmology
MGD dataset

ABSTRACT

Purpose: We aim to present effective diagnostics in the field of ophthalmology and improve eye health. The purpose of this study is to examine the capability of health classification of Meibomian gland dysfunction (MGD) using Keratography 5M and AlexNet method.

Method: A total of 4,609 meibomian gland images were collected from 2,000 patients using Keratography 5M in the hospital. Then, MGD dataset for eyelid gland health recognition was constructed through image pre-processing, labelling, cropping and augmentation. Furthermore, AlexNet network was used to identify the eyelid gland health. The effects of different optimization methods, different learning rates, Dropout methods and different batch sizes on the recognition accuracy were discussed.

Results: The results show that the effect of model recognition is the best when the optimized method is Adam, the number of iterations is 150, the learning rate is 0.001, and the batch size is 80, then, the overall test accuracy of health degree is 94.00%.

Conclusion: Our research provides a reference to the clinical diagnosis or screening of eyelid gland dysfunction. In future implementations, ophthalmologists can implement more advanced learning algorithms to improve the accuracy of diagnosis.

1. Introduction

Dry eye disease (DED) is one of the pervasive diseases of the ocular surface [1–4]. DED affects visual acuity and causes ocular discomfort and other symptoms, leading to changes in the quality of life [5]. Meibomian gland dysfunction (MGD) plays an import roles of DED. It a common clinical condition and a major cause of lip tear deficiency and evaporative dry eye [6–9]. MGD is one of the most common disorders encountered in clinical practice and attracts significant concern among researchers. It is a chronic, diffuse abnormality of the Meibomian glands, commonly characterized by terminal duct obstruction and/or qualitative/quantitative changes in the glandular secretion. This may result in alteration of the tear film and inflammation of the ocular surface, leads to symptoms of eye irritation, even causes destruction to visual function via damaging cornea [10]. The measurement of glandular loss is of significant clinical impact for the diagnosis of MGD. In clinical practice, non-contact infrared meibography is commonly used in the observation and assessment of MGD [11–12]. Meibography was first introduced in the 1980s, when Jester et al. [13] established the use of infrared (IR) light to transilluminate the lid allowing easy observation of the glands. Clinicians normally judge the severity of MG atrophy by observing the image of meibomian gland recorded by infrared camera, it is somewhat subjective which might leads to unaccuracte assessment thus affect the formula in MGD treatment [14–15].

Deep learning is one of the important methods of artificial intelligence [16–17]. It was proposed by Hinton in the year 2006 [18]. Convolutional Neural Network is the most classical calculation method of deep learning, having characteristics such as local connection and weight to value sharing, greatly reducing the data used for learning and reduce the risk of overfitting because of lack of data [19]. Convolutional Neural Network is mainly composed of the input layer, the convolution layer, the pooling layer, the fully connected layer, activation function and dropout layer [20]. The

* Corresponding author.
E-mail address: gaoyingying1968@163.com (Y. Gao).

https://doi.org/10.1016/j.cmpb.2022.106742
0169-2607/

convolution layer is responsible for the extraction of features, the pooling layer is used to reduce the spatial size of the convolved features and the fully connected layer is used to infer final classification. Convolutional Neural Network is continuously undergoing updated and optimized, including AlexNet [21], GoogleNet [22], MobileNets [23], DenseNet [24], EfficientNet [25–26].

In the past, deep learning has been paid increasing attention in the field of ophthalmology [27–30]. Currently, there has been increasing utilization on deep learning for the processing of images of the meibomian gland. In addition, there has been very limited research about meibomian gland health classification by deep learning. Zhou et al. [31] have collected 576 sample data of dry eye patients and constructed a database consisting of 2304 images of meibomian glands. Furthermore, Mask R-CNN method was used for pre-training on Microsoft's COCO dataset. Then, the eyelid conjunctiva and meibomian gland were detected, automatically segmented and the proportion of missing meibomian gland was calculated. However, the health degree of meibomian gland was not further classified. Wang et al. [32] collected 706 meibomian gland images and used ResNet50 model (learning rate attenuation method, 200 epochs) for meibomian gland health recognition, which achieved an overall accuracy of 95.6%, but the amount of data is insufficient, which is not conducive to further research of deep learning in meibomian gland image processing. AlexNet is a traditional method of convolutional neural network. To the best of our knowledge, however, AlexNet is the first model to classify the health level of meibomian gland image, so as providing a refined and convenient method for the diagnosis, treatment and screening of meibomian gland dysfunction. Our motivation is to adopt AlexNet model to explore the possibility of meibomian gland image recognition and explore the optimal network parameters. Actually, there are several parapmeters to affect the performance of health classification of MGD, such as learning rate, batch size, the number of iterations and updated methods. Mastering the parameter adjustment skills can quickly achieve the target accuracy and improve the accuracy.

The rest of the paper is organized into four sections. Source of meibomian gland image and classification basis are introduced in Section 1. Section 2 is a detailed description of construction of MGD dataset. Section 3 is a brief description of research method .Section 4 are experiments and results, mainly including the effect of different parameters on the accuracy. The final conclusion and future research is given in Section 5.

2. Materials

2.1. Meibomian gland

Anatomically, the meibomian glands vertically embedded in the tarsal plates of both the upper and lower eyelid, with the duct terminates in an orifice at the eyelid margin posterior to Marxs line. Meibomian glands secrete lipids into tears, forming a superficial lipid layer that moisturize the ocular surface and prevent excessive evaporation of the tear film. The structure of meibomian gland under infrared camera is shown in Fig. 1, in which A and B are upper eyelids and C and D are lower eyelids.

2.2. Data collection

The meibomian gland images were collected from the 2nd Affiliated Hospital in Fujian Medical University. Photos taken using keratography produced by OCULUS company in German with collection time from January 2015 till December 2020. There are total 4609 meibomian gland images from 2000 patients, all images are in JPG format, which is 1920 pixel x 1080 pixel. This study was approved by the ethics committee of the Second Affiliated Hospital of Fujian Medical University, and the subjects' informed consent was obtained.

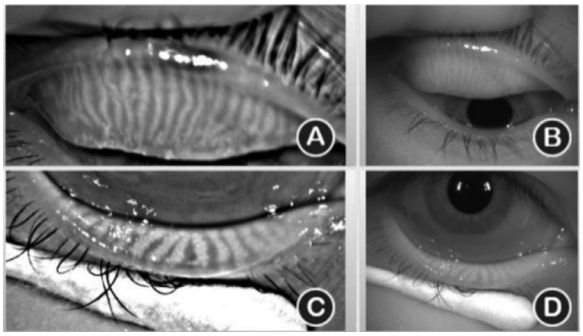

Fig. 1. Upper and lower eyelid of right eye.

Table 1
The grading of meibomian gland health level

Ratio of atrophy(%)	level
0	0 (normal)
0-33	1 (mild)
33-66	2 (moderate)
66	3 (severe)

2.3. Classification criteria of Meibomian gland health

The Keratograph 5M (K5M; Oculus, Wetzlar, Germany) was applied to perform the meibography scans and digitized the meibomian structure. Images of the upper meibomian glands were captured by the K5M on the everting upper eyelid. Generally, based on the MG atrophy ratio (atrophic area / total lid area), the health of meibomian gland is divided into four levels: normal, mild, moderate and severe, according to 4-grade scoring system(0-3) [33]. As shown in Table 1, the atrophy ratio of 0% is normal, 0-33% is mild, 33% - 66% is moderate and more than 66% is severe. In Fig. 2, lines 1 to 4 are image diagrams of meibomian gland health levels from 0 to 3, respectively. Table 1 is the grading of meibomian gland health level.

2.4. Construction of MGD dataset

Dataset of meibomian gland health recognition was built through image preprocessing, labeling, cropping and augmentation, and is named as MGD dataset.

2.4.1. Data source and selections

A total of 4,609 Meibomian gland images were collected from 2,000 patients in the Second Affiliated Hospital of Fujian Medical University from January 2015 to December 2020. Among these images, 2318 images were in left eye and 2291 images were in right eye. 72 images were dropped out because they were not up to standard, such as unclear resolution, serious reflection, incomplete image range, incomplete eyelid turnover, obstruction from eyebrow or other objects. 4537 images that met the requirements were obtained after screening.

2.4.2. Data cropping

The original image contains the images of the upper and lower eyelids, as shown in Fig. 1. In order to improve the recognition accuracy, the upper and lower eyelid images (such as A and C in Fig. 1) are cropped. Because the upper and lower eyelids are regularly distributed in the original image, the x-axis range of the upper eyelid and lower eyelid is (100, 576), (591, 1064), respectively, and the y-axis range of the upper and lower eyelids are (45, 1052).

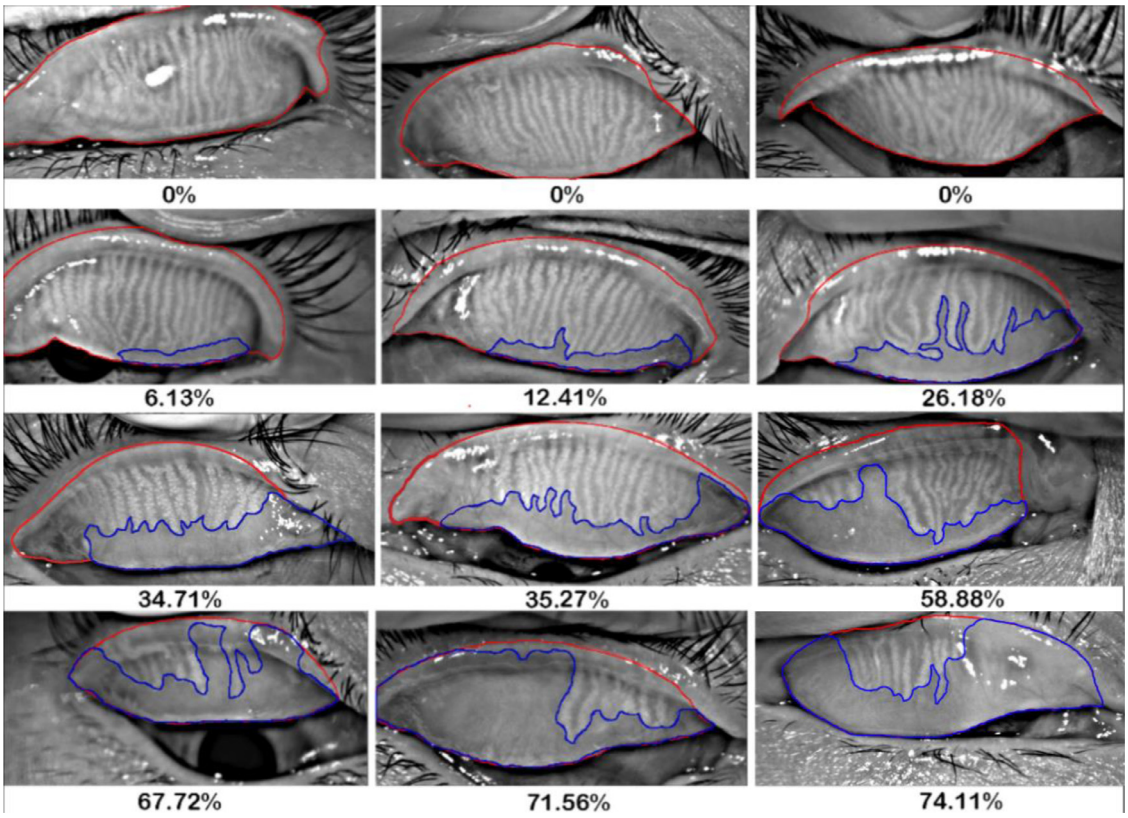

Fig. 2. Health level of meibomian gland

Table 2
Examples of data statistics

No	atrophy	eyelid	proportion	Health level
1	66840	221906	0.3012	1
2	126435	230246	0.5491	2
3	126416	282624	0.4473	2
4364	97788	202749	0.482311	2

4537 images were cropped at one time by python programming, and 9074 upper and lower eyelid images were obtained after segmentation. However, due to image quality problems, 4634 eyelid images were obtained after further checking.

2.4.3. Data annotation

A team of trained individuals labeled and measured the total eyelid and atrophy area by ImageJ image processing software (version No. 1.53E, http://imagej.nih.gov/ij/). The team includes doctors, masters and undergraduate students. ImageJ [34] is a public domain software based on Java for scientific image processing and analysis. It is developed by Wayne Rasband in the National Institutes of Health. When marking, the eyelid range and Meibomian gland atrophy were drew with red and blue line respectively, as shown in Fig. 2. Final annotations were verified by Doctors of Ophthalmology Department. After marking, area of both total eyelid range and its atrophy is automatically calculated, as indicated in Table 2. Furthermore, the proportion of atrophy was calculated and converted to the health level according to Table 1. Totally, there are 4364 samples, among them 364 images are normal, 2822 images are mild, 1038 images are moderate and 140 images are severe.

2.4.4. Data augmentation

Data augmentation is a data processing method that can effectively expand datasets. Due to insufficient samples, normal, moderate and severe images of Meibomian gland are expanded by the third-party library PIL(Python Imaging Library). First, the original images are flipped up and down and left and right; Second, the original image is rotated counter-clockwise; Third, random Gaussian noise is added to the original image (mean value is 0.2 and standard deviation is 0.3); Fourth, the color of the original image is randomly dithered. The RGB color space of the original image is converted to the HSI color space firstly. After randomly disturbing the hue, exposure and saturation in the HSI space, it is converted back to the RGB image.

From 4364 images, 50 images of four different levels are randomly selected as test data. The remaining images are augmented to construct the dataset. Considering the sample balance, 2512 images are obtained after 8 times expansion of normal level images (1 time of up, down, left and right flipping respectively, 4 times of color random jitter and 2 times of random Gaussian noise); 2964 images were obtained after 3-fold expansion of moderate level images (1-fold up and down, 2-fold color random jitter); 1980 images were obtained after 22 times expansion of severe level images (up, down, left and right flip, 5 times random color jitter, 135 °, 225 °, 270 ° and 315 ° counterclockwise rotation, 11 times random Gaussian noise); Images with mild level are enouhg and not expanded.

2.4.5. Final dataset

TFRecords is a binary data packaging format commonly used in tensorflow. Our dataset is packaged into TFRecords files, so as to facilitate the efficient training and evaluation of the model with data loader and transformer APIs in TensorFlow. During the construction of the dataset, four kinds of images are saved in fours files, named with 0, 1, 2 and 3 respectively, and the images in the files are the data of the corresponding labels. Final dataset is disordered and constructed after shuffling the data into new TFRecords file, called as MGD dataset.

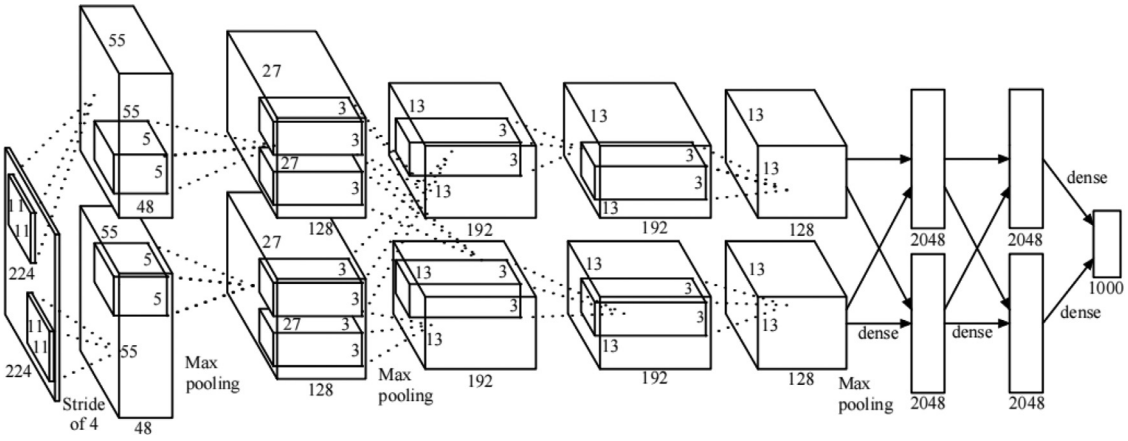

Fig. 3. Structure of AlexNet model

3. Method

In 2012, AlexNet was first proposed by Kriszhevsky and Hinton [21]. The AlexNet network model won the champion of the image classification competition of the large-scale visual recognition challenge (ILSVRC) in that year. The model structure is shown in Fig. 3, including the upper and lower sub networks, with a total of 8 layers (excluding the input layer). AlexNet is based on a forward propagation network, which is one of CNN network and includes 10 layers, such as input layer, convolution layer, response-normalization layer, max-pooling layer and output layer. Toatally, there are 8 convolution layers. The first 5 layers are the convolution layer (including 3 max pooling layers), and the last 3 layers are the full connection layer. The training parameters are 58, 281, 344 (about 60M).

The size of input layer in AlexNet model is a color image of 224 × 224. Both the upper and lower sub networks in the first convolution layer, there are 48 convolutional kernels of size of 11 × 11 with stride of 4 pixels. Then, 48 feature maps of size 55 × 55 are obtained in each sub network. Followed by ReLU unit, local response-normalization(LRN) layers and max-pooling layer(with size 3 × 3, stride of 2), 48 feature maps of size 27 × 27 are outputted in each sub network and taken as the input of the second convolution layer which two sub networks contain 128 kernels of size 5 × 5 with stride of 1 pixels, using the same padding, and output 128 feature maps. After ReLU, LRN and max-pooling process(3 × 3, stride of 2), 128 feature maps with size 13 × 13 are made. The third,fourth, and fifth convolutional layers are connected to one another without any intervening pooling or normalization layers. The third convolutional layer has 384 kernels of size 3 × 3 × 256 connected to the outputs of the second convolutional layer. The fourth convolutional layer has 384 kernels of size 3 × 3 × 192, and the fifth convolutional layer has 256 kernels of size 3 × 3 × 192. The seventh and eighth layers are fully connected layers and have 4096 neurons each. The last layer is the output layer with four neurons that they are four levels of health of eyelid in this research.

4. Results and discussion

4.1. Environment construction

The computer uses Windows10 64-bit operating system, RAM of 16GB, ROM of 8139MB. Using the computer's GPU (NVIDIA GeFore GTX960) and PyCharm (version 2020.3.3) for experimentation, construct Python3.7, TensorFlow2.3.0, Opencv3.4.2 as the environment. Using the self-built MGD data sets that is based on the AlexNet model for health level appraisal. We examine enhancement methods, rate of learning and batch sizes effects on training accuracy and test accuracy [35–37], which are accuracy of training set and test set, respecitvely. In expriment, we train with the training set and after each epoch. The optimizers will always try to update the weights to perfectly classify the training data, the training accuracy will therefore get very high. The test data is data the model has never seen before, and its done after each epoch to show how well the model reacts to data is hasn't seen before, this shows how well the model will improve overtime.

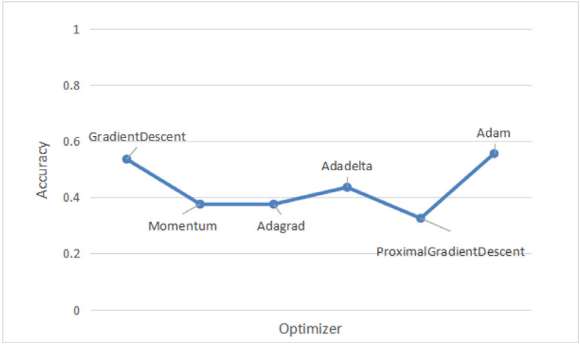

Fig. 4. Effects of optimization methods on accuracy

4.2. Results and discussion

4.2.1. Effects of optimization methods on accuracy

The purpose of neural network learning is to find parameters that make the value of loss function as small as possible [38]. In order to find the optimal weight and parameters, different optimization methods are used to update the parameters of the neural network. Common update optimization methods include Gradient Descent, Momentum, Adagrad, Adadelta, Adam Proximalgradient, etc. However, there is no unified optimization method to solve all problems, which can only be determined through experiment according to specific application scenarios. Normally, it is found that as the number of training iterations increases for each algorithm, the test accuracy of the classification on the MGD image test set is also improving, but not Increase infinitely. After lots of expriments, the number of iterations is set to 50, the learning rate is set to 0.1, the batch size is set to 50, and the ratio of training set to test set is 10:1. The relationship between accuracy and different optimization methods is shown in Fig. 4. The accuracy obtained by all optimization methods is not high, which is related to other hyper parame-

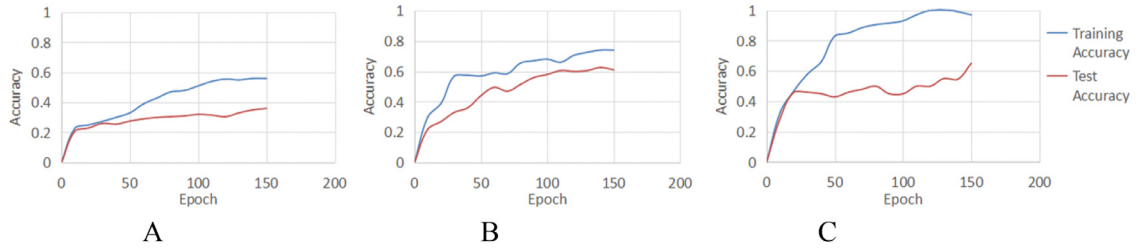

Fig. 5. Relationship between accuracy and learning rate A learning rate is 0.1. B learning rate is 0.01. C learning rate is 0.0001.

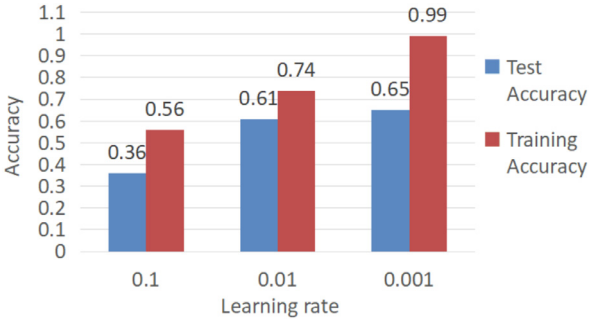

Fig. 6. Highest accuracy under different learning rates

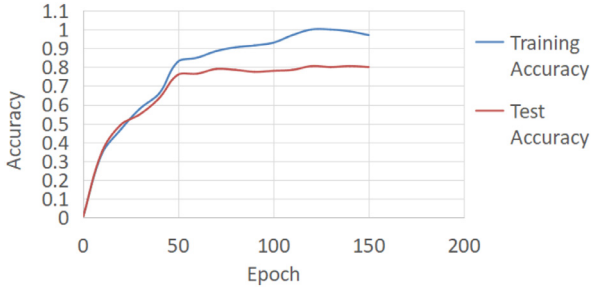

Fig. 7. Effects of Dropout on accuracy

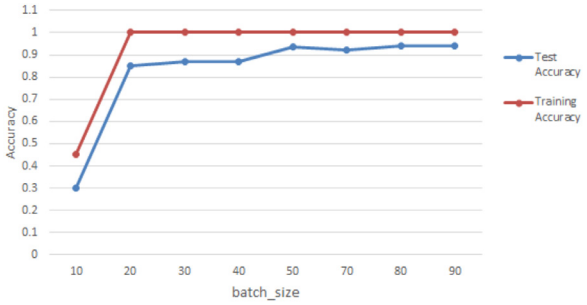

Fig. 8. Effects of batch size on accuracy

ter settings. From Fig. 4, the result of Adam optimization method is better than other optimization methods. Therefore, the Adam optimization method is adopted in the following experiment.

4.2.2. Effects of learning rates on accuracy

Learning rate is is a hyper parameter, a key parameter of training neural network, which can control the adjustment degree of network weight in the loss gradient. he lower the learning rate, the slower we are going downhill. If the learning rate is too large, gradient decent can overshoot the minimum. It may fail to converge, or even diverge**.** The number of iterations is one of the most important hyper-parameters. In experiment, we get higher training accuracy with increasing iterations. Yet, it took more time to achieve higher accuracy. We balance the time cost and accuracy. In order to explore the optimal learning rate, the number of iterations is fixed to150, the batch size is set to 50, and the ratio of training set to test set is 7:3. The training accuracy and test accuracy when learning is 0.1, 0.01 and 0.001 are shown in A, B,C in Fig. 5 respectively. The highest training accuracy and test accuracy of different learning rates are shown in Fig. 6. It can be seen from Fig. 6 that the training accuracy and test accuracy increase with the decrease of learning rate. When the learning rate is 0.001, the training accuracy and test accuracy are the highest, which are 0.99 and 0.65 respectively. In subsequent experiments, the learning rate is set to 0.001. However, over-fitting occurs as shown in Fig. 6, that means, the training accuracy is high, but the test accuracy is low. Then, dropout method is added to the model to deal with the overfitting.

4.2.3. Effects of dropout on accuracy

In training, parts of neurons (except the output layer) are randomly dropped according to a certain probability. That is, the deleted neurons do not work during the pre-training; However, all neurons recover and transmit loss during the test. In general, it is the best to set the retention rate of neurons in the hidden layer 0.5, because the randomly generated network structure is the most diverse [39]. In order to explore the influence of dropout on accuracy, the number of iterations is set to 150, the batch size is set to 50, and the ratio of training set to test set is 7:3. The experimental results after dropout are shown in Fig. 7. The training accuracy approaches 1.0 at the 120th epoch, and the maximum test accuracy is increased to 80.5%. Compared with C in Fig. 5, the gap between training accuracy and test accuracy is reduced, that is, the overfitting is suppressed. Randomly discarding neurons can be considered as resampling features, reducing the amount of features and improving the generalization ability.

4.2.4. Effects of batch size on accuracy

It is an effective way to select a small batch of data from the whole sample during the training of neural network. This part of data is considered as the approximate value of all training data. It is an iteration to update weights and biases for the small batch. Yet, batch size has a great impact on network optimization. In order to explore the influence of batch size on accuracy, the number of iterations is set to 150, the learning rate is set to 0.001, and the ratio of training set to test set is 7:3. The batch size is taken from {10, 20, 30, 40, 50, 70, 80, 90}. The impact of different batch sizes on accuracy is shown in Fig. 8. When the batch size is 80, the training accuracy reaches the maximum value of 94%.

4.3. Test effect of optimal parameters

In summary, the optimization method of Adam, the number of iterations of 150, the learning rate of 0.001 and the batch size of 80 are the optimal parameters for AlexNet model to identify

Table 3
Confusion matrix of the optimal parameters

Actual	Predict			
	0	1	2	3
0	49	0	0	1
1	2	44	2	2
2	0	2	48	0
3	0	0	3	47

meibomian gland health. Taking MGD as the dataset, the MGD-AlexNet model is generated through training and saved as a h5 file. 200 pictures are tested with this model, 50 pictures of each type of health degree. The confusion matrix of the test is shown in Table 3. Among the normal grades, 49 images were correctly identified, and one of them was misjudged as severe grade, and the correct recognition rate of this grade was 98%; Among the mild health grades, 44 were correctly identified, and there are two images were wrongly divided into every normal, moderate and severe grade. The correct recognition rate of this grade was 88%; Among the moderate grades of health, 48 were correctly identified, and 2 were misjudged as mild grades. The correct recognition rate of this grade was 96%; Among the severe health grades, 47 were correctly identified, and 3 were misjudged as moderate. The correct recognition rate of this grade was 94%. The test accuracy of overall health recognition is 94%. In fact, in manual interpretation, the normal and severe grades are relatively easy to judge, but due to the close atrophy of mild and moderate grades, it is difficult to distinguish them manually. Perhaps some kind of predictive control algorithms [40] can be used to achieve the optimal parameters pertaining to our neural network in future studies.

5. Conclusion

MGD dataset for meibomian gland health recognition was firstly constructed through image preprocessing, labeling, cropping and augmentation. This dataset includes 4364 original images and 200 testing images. These images are collected from Second Affiliated Hospital of Fujian Medical University, 4609 meibomian gland images of 2000 patients from January 2015 to December 2020. In this paper, a total of 4364 MGD images are used for experiments, among them 364 images are normal, 2822 images are mild, 1038 images are moderate and 140 images are severe. 50 images of are randomly selected as test data. The total training set is 4314. There are more 10000 images in final dataset after data augmentaion. This dataset is beneficial for the training and further experiment of other deep learning methods. Although the dataset is built, it needs to collect images from different countries, regions and ages to increase the image sample size and improve data diversity. The datasets of the four types of MGD images constructed in this paper need to be greatly expanded, and the collection of a large number of MGD images is a necessary work for further research, including images from different regions, different countries.Moreover, it takes time and effort to set up dataset manually through ImageJ software. Future research should focus on image segmentation algorithm or deep learning method to automatically extract meibomian gland and its atrophic part, so as to enhance the intelligent recognition ability of meibomian gland health.

The proposed AlexNet model was successfully applied to meibomian gland health recognition using self-built MGD dataset. Four levels of health of eyelid were automatically predicted without any manual work. The model gets high performance when the optimization method is Adam, the number of iterations is 150, the learning rate is 0.001 and the batch size is 80. In this case, accuracy of four levels was 98%, 88%, 96%, and 94%. The test accuracy of overall health recognition is 94%. It provides a demonstration for the cross research of artificial intelligence and ophthalmology. However, it is unclear to know how the model effectively identifies different levels of eyelid images. In the next step, it is urgent for the researchers to reveal how it works. At the same time, multi computers and multi GPU can be processed in parallel, so as to reduce the training time. And it is also a recent research hotpot how to automatically solve the problem of parallel policy selection from TensorFlow.

Declaration of Competing Interest

There are no conflicts of interest to disclose for publication of this paper.

Acknowledgments

The work was supported by Science and Technology Program of Quanzhou No. 2021N180S and No. 2021CT0010. This research is partly supported by the Project of Natural Science Foundation of Fujian Province under Grant No. 2020J01785. The authors also acknowledge the support by Fujian Provincial Key Laboratory of Data-Intensive Computing, Fujian University Laboratory of Intelligent Computing and Information Processing, and Fujian Provincial Big Data Research Institute of Intelligent Manufacturing.

References

[1] J.P. Craig, et al., TFOS DEWS II report executive summary, Ocular Surf. 15 (2017) 802–812.
[2] F. Stapleton, et al., TFOS DEWS II epidemiology report, Ocular Surf. 15 (2017) 334–365.
[3] J.P. Craig, et al., TFOS DEWS II definition and classification report, Ocular Surf 15 (2017) 276–283.
[4] M.E. Stern, J. Gao, K.F. Siemasko, R.W. Beuerman, S.C. Pflugfelder, The role of the lacrimal functional unit in the pathophysiology of dry eye, Eye Res. 78 (2004) 409–416.
[5] K.K. Nichols, et al., The international workshop on meibomian gland dysfunction: executive summary, Investig. Ophthalmol. Vis.Sci. 52 (2011) 1922–1929.
[6] Y. Chen, L.I. Sheng, M.A. Ming, Therapeutic effect of intense pulsed light combined with long pulse width Nd:YAG laser on facial telangiectasia, Chin. J. Aesthet. Med. (2019).
[7] H. Wu, Z. Lin, F. Yang, et al., Meibomian Gland Dysfunction Correlates to the Tear Film Instability and Ocular Discomfort in Patients with Pterygium, Sci. Rep. 7 (2017) 45115.
[8] J. Xiao, M.Y. Adil, J. Olafsson, et al., Diagnostic test efficacy of Meibomian gland morphology and function, Sci. Rep. 9 (1) (2019) 17345.
[9] Y. Eom, K.S. Na, H.S. Hwang, et al., Clinical efficacy of eyelid hygiene in blepharitis and Meibomian gland dysfunction after cataract surgery: a randomized controlled pilot trial, Sci. Rep. 10 (1) (2020) 11796.
[10] Chinese Branch of Asian Dry Eye Association, Ophthalmology group of ophthalmology professional committee of cross strait medical exchange association. Consensus of experts on diagnosis and treatment of Meibomian gland dysfunction in China, Chin. J. Ophthalmol. 63 (9) (2017) 657–661.
[11] S. Srinivasan, K. Menzies, L. Sorbara, et al., Infrared Imaging of Meibomian Gland Structure Using a Novel Keratograph, Optomet. Vis. Sci. 89 (5) (2012) 788.
[12] A.S. Wong, et al., Comparison of meibomian gland dropout using two infrared imaging devices, Contact Lens Anterior Eye 42 (3) (2019) 311–317.
[13] J.V. Jester, L. Rife, D. Nii, et al., In vivo biomicroscopy and photography of Meibomian glands in a rabbit model of meibomian gland dysfunction, Invest. Ophthalmol. Vis. Sci. 22 (5) (1982) 660.
[14] A. Reiko, et al., Objective image analysis of the meibomian gland area, Br. J. Ophthalmol. 98 (6) (2014) 746–755.
[15] M. Randon, V. Aragno, R. Abbas, et al., In vivo confocal microscopy classification in the diagnosis of Meibomian gland dysfunction, Eye 33 (5) (2019) 754–760.
[16] X.X. Luo, S.Y. Xu*, H. Yan, Application of deep belief network in forest type identification using hyperspectral datas, Adv. Sci., Technol. Eng. Syst. J. 5 (6) (2020) 1554–1559.
[17] X.X. Luo, S.Y. Xu*. Forest mapping from hyperspectral image using deep belief network //Pengfei Wang. 2019 15th International Conference on Mobile Ad-hoc and Sensor Networks (MSN). Shenzhen:IEEE, 2019:395-398.
[18] G.E. Hinton, R.R. Salakhutdino, Reducing the dimensionality of data with neural networks, Science 313 (5786) (2006) 504–507.
[19] W. Wu. Deep Learning Practice. Beijing: Electronic Industry Press, 2020, 89.
[20] X.X. Luo, W. Zeng, X.Y. Chen, et al., Research on remote sensing images processing using deep learning, J. Quanzhou Normal Univ. 35 (180) (2017) 35–41.
[21] A. Krizhevsky, I. Sutskever, G.E. Hinton, ImageNet classification with deep convolutional neural networks, Commun. ACM 60 (6) (2017) 84–90.

[22] C. Szegedy, W. Liu, Y.Q. Jia et al. Going deeper with convolutions. Proc of the IEEE Conference on Computer Vision and Pattern Recognition. 2015. 1-12.
[23] A.G. Howard, M.L. Zhu, B. Chen, et al. MobileNets: efficient convolutional neural networks for mobile vision applications. arXiv preprint arXiv:1704.04861, 2017.
[24] G. Huang, Z. Liu, L. Maaten, Densely connected convolutional networks, CVPR (2017) 4700–4708.
[25] M. Tan, Q.V. Le. EfficientNet: rethinking model scaling for convolutional neural networks. 2019.
[26] M. Tan, Q.V. Le. EfficientNetV2: smaller models and faster training. 2021.
[27] D. Ting, L.R. Pasquale, L. Peng, et al., Artificial intelligence and deep learning in ophthalmology, Br. J. Ophthalmol. 103 (2) (2018) 167–175.
[28] R. Gargeya, T. Leng, Automated identification of diabetic retinopathy using deep learning, Ophthalmology (2017) 962–969.
[29] P.S. Grewal, O. Faraz, R. Uriel, et al., Deep learning in ophthalmology: a review, Can. J. Ophthalmol. 53 (2018) 309–313.
[30] D. Ting, L. Peng, A.V. Varadarajan, et al., Deep learning in ophthalmology: The technical and clinical considerations, Prog. Retin. Eye Res. (2019).
[31] Y.W. Zhou, H. Yu, Y.B. Zhou, et al., An advanced imaging method for measuring and assessing Meibomian glands based on deep learning, Chin. J. Ophthalmol. 56 (10) (2020) 774–779.
[32] J.Y. Wang, T.N. Yeh, R. Chakraborty, et al., A deep learning approach for Meibomian gland atrophy evaluation in meibography images, Transl. Vis. Sci. Technol. 8 (6) (2019) 1–11.
[33] R. Arita, K. Itoh, K. Inoue, S. Amano, Noncontact infrared meibography to document age-related changes of the Meibomian glands in a normal population, Ophthalmology 115 (2008) 911–915.
[34] J. Schindelin, I.A. Carreras, E. Frise, et al., Fiji: an open-source platform for biological-image analysis, Nat. Methods 9 (2012) 676–682.
[35] Y. Yu, Y. Zhou, Y. Yang, et al. Automatic identification of Meibomian gland dysfunction with meibography images using deep learning. 2021.
[36] S. Chakraborty, S. Paul, K.M.A. Hasan. A transfer learning-based approach with deep CNN for COVID-19- and pneumonia-affected chest x-ray image classification. 2022.
[37] J.M. Czum, Dive into deep learning, J. Am. Coll. Radiol. 17 (5) (2020) 1–10.
[38] K.K.L. Wong, G. Fortino, D. Abbott, Deep learning-based cardiovascular image diagnosis: a promising challenge, Fut. Gener. Comput. Syst. 110 (2020) 802–811.
[39] J. Patterson, A. Gibson, Deep learning[M], Boston: O'Reilly Media (2017) 117–163 Inc.
[40] Z.H. Tang, Y.Y. Li, X.Y. Chai, H.Y. Zhang, S.X. Cao, Adaptive nonlinear model predictive control of NOx emissions under load constraints in power plant boilers, J. Chem. Eng. Jpn. 53 (1) (2020) 36–44, doi:10.1252/jcej.19we142.